Investigation of peeling-ballooning stability prior to transient outbursts accompanying transitions out of H-mode in DIII-D

D. Eldon,[1,2,a)] R. L. Boivin,[3] R. J. Groebner,[3] T. H. Osborne,[3] P. B. Snyder,[3] A. D. Turnbull,[3] G. R. Tynan,[1] J. A. Boedo,[1] K. H. Burrell,[3] E. Kolemen,[2] L. Schmitz,[4] and H. R. Wilson[5]
[1]*University of California San Diego, 9500 Gilman Dr., La Jolla, California 92093-0964, USA*
[2]*Princeton University, Princeton, New Jersey 08543, USA*
[3]*General Atomics, P.O. Box 85608, San Diego, California 92186-5608, USA*
[4]*University of California Los Angeles, Los Angeles, California 90095-7099, USA*
[5]*University of York, Heslington, York YO10 5DD, United Kingdom*

(Received 17 February 2015; accepted 27 April 2015; published online 14 May 2015)

The H-mode transport barrier allows confinement of roughly twice as much energy as in an L-mode plasma. Termination of H-mode necessarily requires release of this energy, and the timescale of that release is of critical importance for the lifetimes of plasma facing components in next step tokamaks such as ITER. H-L transition sequences in modern tokamaks often begin with a transient outburst which appears to be superficially similar to and has sometimes been referred to as a type-I edge localized mode (ELM). Type-I ELMs have been shown to be consistent with ideal peeling ballooning instability and are characterized by significant (up to ∼50%) reduction of pedestal height on short (∼1 ms) timescales. Knowing whether or not this type of instability is present during H-L back transitions will be important of planning for plasma ramp-down in ITER. This paper presents tests of pre-transition experimental data against ideal peeling-ballooning stability calculations with the ELITE code and supports those results with secondary experiments that together show that the transient associated with the H-L transition is not triggered by the same physics as are type-I ELMs. © *2015 AIP Publishing LLC*. [http://dx.doi.org/10.1063/1.4919942]

I. INTRODUCTION

High confinement or H-mode is an attractive regime of tokamak operation as it allows operation at higher temperature and density than L-mode or Ohmic operation.[1,2] In H-mode, additional stored energy builds up behind a transport barrier which is present in the last ∼5% of closed flux surfaces. This inventory of heat and particles must necessarily be released during shutdown of the device. The transport barrier typically forms rapidly and it can also dissipate abruptly. The resulting outflow of plasma may have deleterious effects on the plasma facing components of ITER or a reactor and must be better understood and possibly mitigated.

H- to L-mode back transitions have been observed to be accompanied by a sudden drop in stored energy and pedestal height, as shown in Fig. 1 by time traces of these and other parameters and in Fig. 2 by profiles before and after the initial spike (4402 ms, Fig. 1) associated with the H-L transition sequence. This event will be referred to as the transient. Depending on how the energy released by the transient scales with machine size, this event could pose a problem for next step devices such as ITER. The transient is superficially similar to a large type-I edge localized mode (ELM). Although benign in modern tokamaks, models of peeling-ballooning driven type-I ELMs indicate that these events can cause high levels of wall erosion in ITER and must be controlled.[3–6] If the transient is a peeling-ballooning unstable type-I ELM,[7,8] then existing ELM models may be applicable and could provide estimates of heat loads or guide mitigation strategies. This paper presents results from DIII-D[9] which indicates that these H-L back transition transients are not driven by ideal peeling-ballooning modes.

In the H-mode example shown in Fig. 1, which is typical of the cases examined in this paper, neutral beam injection (NBI) is turned on at the start of the plot range and soon triggers the L-H transition, resulting in ELM-free H-mode beginning at 3540 ms. The H-mode develops until ELMs are driven starting at 3770 ms. Beams are reduced to diagnostic levels at 4200, and ELMs stop at 4230 ms. An ELM-free period persists until 4402 ms, when the back transition sequence begins with the large transient in D_α emission [Fig. 1(a)]. Figure 2 shows the relaxation of the pedestal as a result of the transient at 4402 ms: the height of the pedestal (especially in density) is greatly reduced between the slices at 4401 and 4411 ms.

The remainder of the paper is organized as follows: background information in Sec. II, including descriptions of peeling-ballooning physics and ELITE; details of the experimental setup in Sec. III; stability analysis description and results in Sec. IV; secondary experiments in Sec. V; and discussion and conclusion in Secs. VI and VII.

II. BACKGROUND

A. Tokamak confinement regime transitions

The H-mode transport barrier is a self-reinforcing condition where a steep pressure gradient exists in a narrow region

a)Author to whom correspondence should be addressed. Electronic mail: deldon@princeton.edu

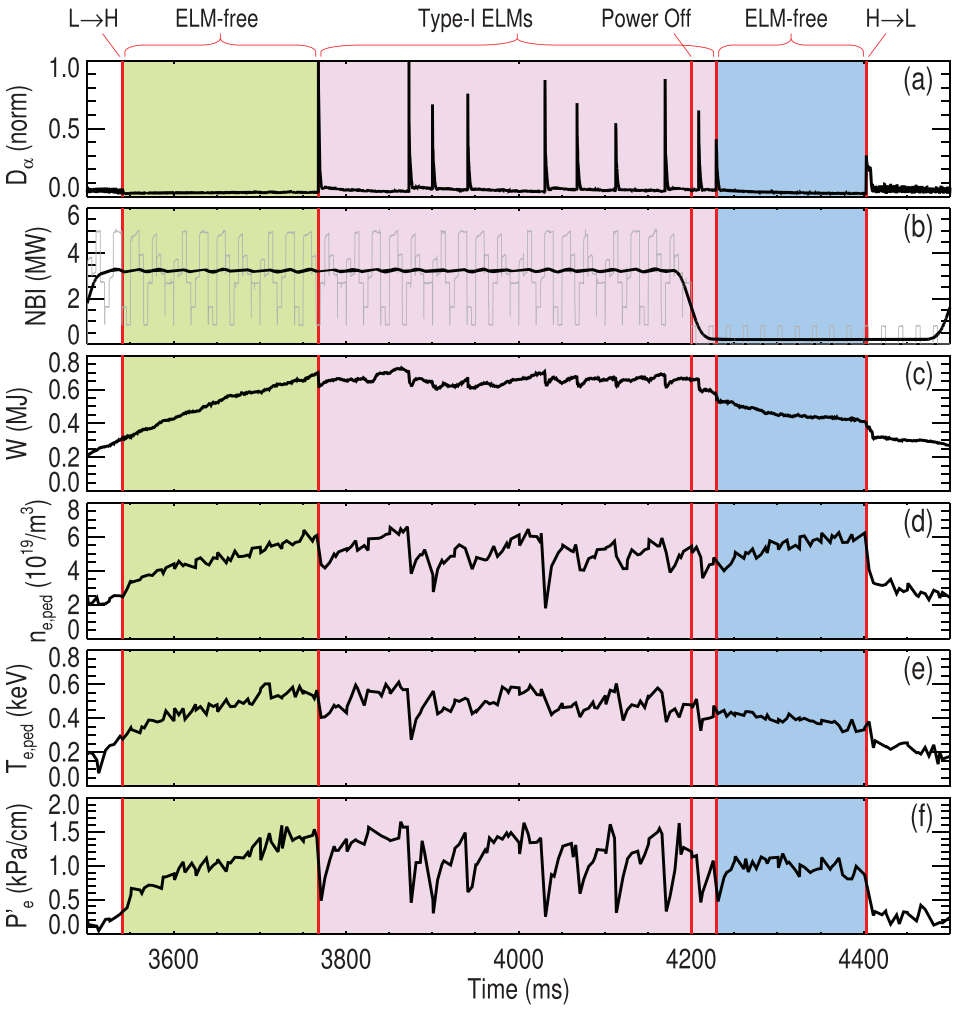

FIG. 1. Evolution of a plasma leading up to a H-L back transition. Critical times are marked with vertical red lines; the last one (4402 ms) is the start of the back transition sequence. (a) D_α emission measured on a chord ending on the outer strike point on the divertor shelf, (b) NBI average power; several beams are modulated for diagnostic reasons. Smoothed power is plotted in bold, (c) plasma stored energy from MHD calculation, (d) pedestal electron density from tanh fit to Thomson scattering data. (e) Corresponding pedestal electron temperature. (f) Pedestal pressure gradient from tanh fit.

of reduced turbulent transport. The ion pressure gradient drives a radially inward electric field in the same narrow region, and the localization of the field results in rapid radial variation, or shear, in the $E \times B$ drift velocity. This shear suppresses turbulent transport by tearing eddies apart and reducing their radial correlation length, thus allowing the steep gradient to exist.[10] In a spontaneous back transition due to a reduction in input power, stored energy would be expected to decay until power flux across the boundary could no longer sustain the transport barrier. The pressure gradient would relax, resulting in a reduction in the $E \times B$ shearing rate and allowing turbulence to re-emerge, and the plasma would no longer be in H-mode. The exact mechanics of how this happens and which instabilities are involved will determine power fluxes and heat loading on plasma facing components during back transitions.

H-L transitions may proceed in various ways, sometimes including a period of oscillations or "dithering" which is characterized by a series of small, rapid D_α spikes. The experiments in this paper were arranged with the goal of producing very long transition sequences, and as a result, extended periods of dithering are present in the discharges studied here. The large transient event in question precedes the dithering and will be considered to be the start of the H-L transition sequence.

Previous studies on H-L transitions[11–15] have focused on transition thresholds, ramp-down procedures, head loads, control systems, and timescales. Forward and backward transitions and dithering are modeled in some work on the basis of thresholds and changes in power flux following confinement changes. This paper will focus on the physical mechanism of the initial large transient (e.g., Fig. 1 at 4402 ms) which is associated with back transitions: is the onset of the H-L transition sequence caused by ideal peeling-ballooning (P-B) instability?

B. Equilibrium reconstruction with EFIT

In this work, a linear MHD stability analysis is performed using equilibria produced by the EFIT code[16] as inputs. The equilibria are based on measurements from magnetic probes[17,18] and the experimental pressure profile as measured by high resolution Thomson scattering[19] and charge exchange recombination (CER) spectroscopy.[20,21] These data are used to constrain solutions to the Grad-Shafranov equation and find a self-consistent solution for the magnetic field, current, and pressure everywhere. Because the parallel current is not directly measured in the edge barrier region, calculated bootstrap current,[22,23] together with Ohmic current, is used to reconstruct the current profile in this region, as is standard practice in edge stability analysis (e.g., Ref. 24). The calculated Ohmic + bootstrap current profile is provided to EFIT, which attempts to find a solution

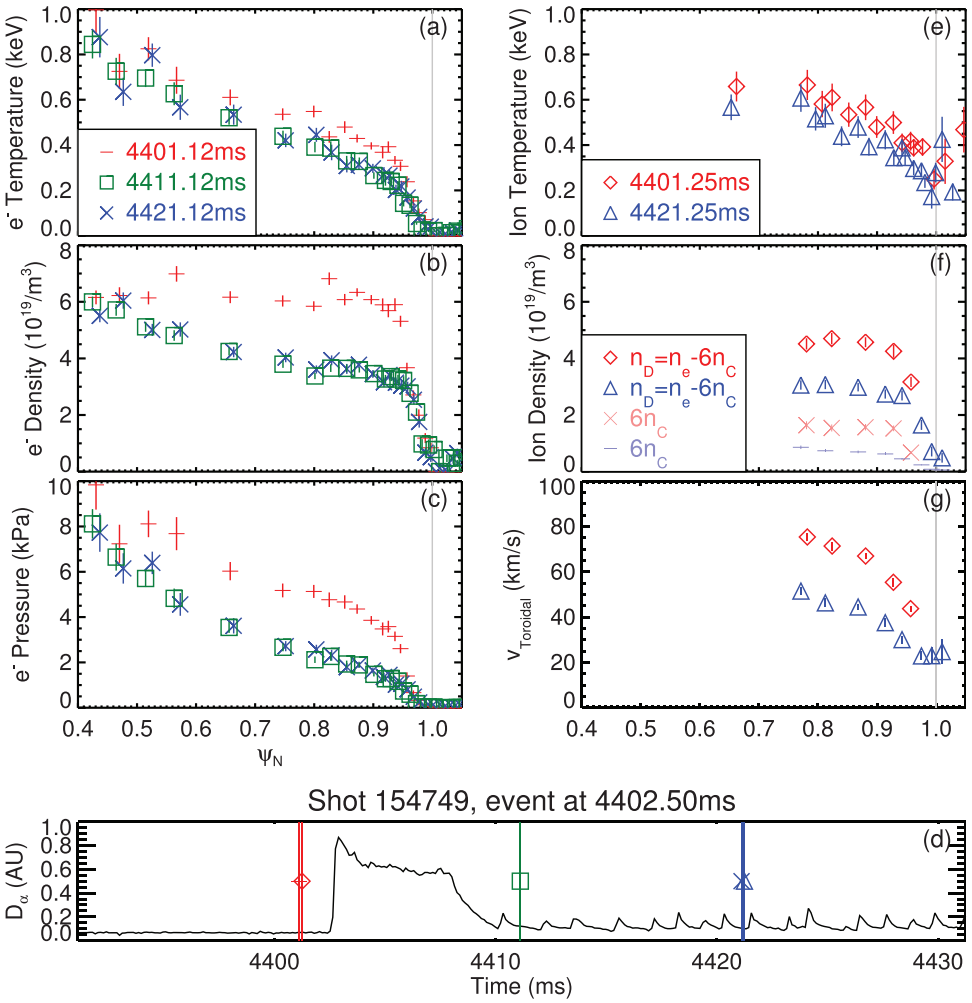

FIG. 2. Relaxation of the pedestal as a result of the transient event at the beginning of the back transition sequence. A time slice immediately before the event is shown with red dashes (Thomson scattering) and diamonds [charge exchange recombination (CER) spectroscopy], 10 ms later (after the event) with green squares (Thomson scattering), and ~20 ms after the first slice with blue Xs (Thomson scattering) and triangles (CER). (a)–(c) Electron temperature, density, and pressure, (d) D_α from the outer strike point on the divertor shelf with vertical lines marking the times in the profiles above, (e) ion temperature, (f) fully stripped carbon density from CER (faded dashes and Xs) and calculated deuterium density (diamonds and triangles), and (g) toroidal rotation (CER).

that is consistent with both the calculated profile and the data from magnetic probes. Hyperbolic tangent and spline fits are used to prepare temperature and density measurements to form the pressure constraints used in the reconstruction.

It is common practice when performing edge stability analysis to perturb the input EFITs by varying the pedestal pressure gradient p' and current J. By doing so, a map of stability in $p' - J$ space may be made and it is possible to evaluate how close the conditions are to instability. When varying the edge values of pressure and current, the values of these parameters in the core are typically adjusted to maintain constant total pressure/current. The boundary remains essentially the same, although minor perturbation to the X point may occur.

The process of fitting temperature and density profiles to form constraints on EFIT is not entirely automatic. In most cases, human judgment is needed to adjust the fits, such as changing knots in the splines. It has been found that the same input data will return slightly different final results when fit by different experienced users. These differences have been characterized and accounted for in the uncertainty in the plasma operating point reported on the stability maps calculated with ELITE. Also note that temperature and density can experience independent errors, which means independent variation in p' and J. Therefore, it is useful to perturb the kinetic EFIT by varying both pressure and current rather than only modifying the pressure profile and adjusting the current profile to match. There is a continuum of consistent current profiles for any pressure profile, defined by the separate contributions of temperature and density to the pressure.

C. Peeling-ballooning model

While the steep pressure gradient at the edge of the plasma increases average temperature, density, and confinement time in H-mode, the pressure gradient provides a source of free energy for ballooning modes, and it also drives bootstrap current[22,25] which is a source of energy for peeling modes. In the magnetic geometry of a tokamak, these modes often interact and the coupled peeling-ballooning mode at intermediate toroidal mode number n is commonly believed to be the limiting constraint on pedestal height.[7] P-B stability was first studied in the local high-n limit, and it was later

found that higher order non-local terms are required for agreement with observation.[7]

Ballooning modes are a type of interchange instability, driven by pressure gradients and unfavorable curvature. The drive is essentially similar to the Rayleigh-Taylor instability, with centrifugal force taking the place of the external or gravitational force.[26] Hence, the drive only exists on the low field side of the plasma and the curvature is stabilizing on the high field side. Ballooning modes are structured such that their amplitude is greater in the region of destabilizing curvature and lower in the region of stabilizing curvature. Therefore, energy is expended in the bending of magnetic field lines and details of the magnetic configuration affect the stability of this mode. In the local high-n limit, high enough pressure gradient $[(dp/dr) \sim (1/Rq^2) \times (B^2/\mu_0)$ (Ref. 31)] can overcome the stabilizing effects of field line bending and result in an ELM. With non-local (finite-n) effects, the width of the edge barrier is also important for quantitative evaluation of stability.[7,24]

Peeling or external kink modes are driven by edge current and are most unstable when a resonant surface is just outside the plasma.[28–31] For a tokamak with circular cross section and in the large aspect ratio limit, energy available for a kink displacement ξ is $\sim B_\theta(nq-m)(dJ_\phi/dr)\xi^2$, where B is the magnetic field, n and m are the toroidal and poloidal mode numbers, and q is the safety factor. Physically, the drive arises from the torque on a flux tube due to the perturbed $J \times B$ force in the presence of a current gradient.[31] Kinking is stabilized by the energy penalty for bending magnetic fields $\sim B'^2$, where $\vec{B}' = \vec{\nabla} \times (\vec{\xi} \times \vec{B}_\theta)$ is the perturbed magnetic field. In the limit where the resonant surface approaches the plasma edge, the perturbation ξ becomes increasingly localized near the surface: $\xi = \xi_a(m-nq_a)/(m-nq)$, where the subscript a denotes quantities at the plasma surface.[31] Such localization gives the peeling mode its name: the edge layer "peels" away. Peeling dominated modes often drive smaller ELMs as their radial penetration depth is typically short, and they tend to occur at lower density where the bootstrap current is higher.[7] In practice, the edge-localized kink drive is usually more important than the surface term, and large ELMs or the edge harmonic oscillation (EHO) are frequently observed at the current-driven stability limit.[7,24]

Tokamak geometry and common shaping effects break the symmetry that would be found in a simple cylinder, resulting in the coupling of poloidal Fourier harmonics with the same toroidal mode number (m couples to $m+b$, where b is some integer). Coupling of the ballooning and external kink modes has the effect of reducing overall stability as the coupled mode can be unstable when ideal ballooning and peeling would be independently stable.[7,33] Coupling tends to be strongest at intermediate toroidal mode number n close to 20 and is affected by boundary shape and aspect ratio.[3,7] In particular, increases in upper triangularity for a diverted plasma with a dominant X-point at the bottom tend to reduce coupling and increase the stable area in $p' - J$ space. Figure 3, adapted from Figure 5 of Ref. 7, shows a schematic of the typical effect of increasing upper triangularity in a lower single-null discharge: the original stable area at low

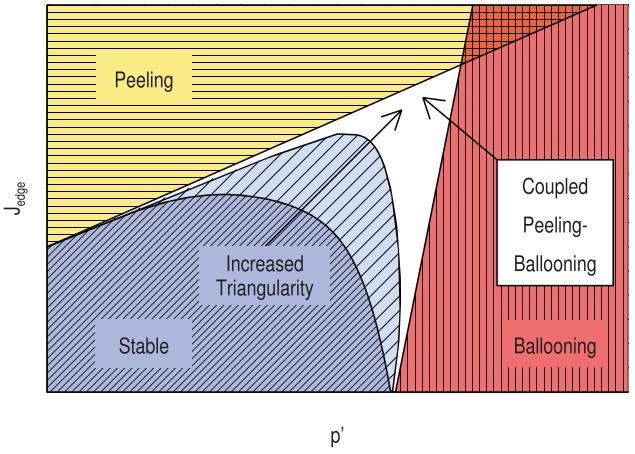

FIG. 3. P-B stability schematic in $p' - J$ space. Ballooning modes (red, vertical hash) are excited by high pressure gradients. Peeling modes (yellow, horizontal hash) are excited by edge current. Coupled peeling-ballooning modes (white, no hash) can be excited under conditions to which peeling and ballooning are independently stable. Increasing triangularity helps stabilize the coupled modes (pale blue, coarsely spaced diagonal hash). Some parameter ranges are stable without strong shaping (darker blue, finely spaced diagonal hash). Adapted from Fig. 5 of Ref. 7.

triangularity (in dark blue) expands until the light blue area is also stable. Higher n modes tend to be stabilized by magnetic shear or finite Larmor radius effects. Steeper pressure gradients have a stabilizing effect on peeling modes, and edge current tends to stabilize ballooning modes and hence the purely peeling and purely ballooning branch boundaries have the slopes shown in the figure. Edge current is generated by the bootstrap current.[22] There is a separate dependence on temperature and density due to the collisional dependence of the bootstrap current.[7]

D. ELITE

In order to efficiently study the DIII-D discharges reported in this paper, including realistic geometry and non-local effects, the ELITE code was used to solve the linear MHD stability against P-B modes.[7,30,32] ELITE solves an expansion of the ideal MHD equations to the accuracy required to study peeling-ballooning mode thresholds and to calculate growth rates for experimental or hypothetical equilibria. It employs an analytical expansion and numerical methods which allow it to very efficiently study intermediate to high n modes which are thought to cause type-I ELMs. The MHD energy equations are expanded in $1/n$ to second order and the code solves a set of Cauchy-Euler equations for Fourier mode amplitudes. ELITE is further optimized to improve efficiency: modes are concentrated around their rational $(m = nq)$ surfaces, so only a subset of poloidal harmonics are significant at any given point and the rest can be neglected. An analytic expansion of the Grad Shafranov equation is performed to allow a more precise calculation of local (same flux surface) quantities and their derivatives. Finally, the grid for evaluating the finely varying Fourier modes is separated from the grid for the equilibrium, which can be much coarser. The expansion in $1/n$ means that ELITE is appropriate for n values of at least 4 or 5, and typical type-I ELMs have $n \sim 5-30$.

The ideal model does not account for stabilization by diamagnetic and finite Larmor radius effects, and it is common practice to compare the calculated growth rates to $\omega_{*i}/2$,[34] where $\omega_{*i} = k(T_i/ZeBn_i)n'_i$ is the ion diamagnetic drift frequency, $k = (2\pi/\lambda)$ is the wavenumber, n_i and T_i are ion density and temperature, Z is charge state, and e is the elementary charge. With this diamagnetic threshold $(\gamma_{MHD} > \omega_{*i}/2)$, ELITE does successfully predict ELM onset in most regimes, including large type-I ELMs.[7] An exception is high density type-III ELMs, which may involve kinetic or resistive effects.[7] In fact, ω_{*i} is subject to significant variation over the width of the pedestal. An effective value ω_{*eff} for diamagnetic frequency may be obtained from a two-fluid calculation with the BOUT++ code;[35] the condition for instability is then $\gamma_{MHD} > \omega_{*eff}/2$. However, the BOUT++ calculation of ω_{*eff} is very similar to the peak ω_{*i} for $n < 15$,[35] and so the simple value of ω_{*i} was used in this work.

ELITE has been successfully benchmarked against GATO[36] for $4 \leq n \leq 10$ and against MISHKA,[37] MARG2D,[38] M3D-C^1,[39] BOUT++,[40] and NIMROD[41] for $n \geq 5$ up to at least 20 but as high as $n = 100$ for MARG2D. Further evidence of ELITE's predictive power comes from the success of the EPED model, which combines ELITE calculations on sets of model equilibria with kinetic ballooning mode constraints to predict the pedestal height and width.[24,35]

E. Resonance and edge *q*

An additional consideration for ideal stability analysis near the edge of the plasma is the value of the safety factor at the edge of the model plasma, q_a. The model in ELITE includes an ideal plasma and an ideal vacuum with a sharp transition between them. In reality, the high temperature and highly conductive (Spitzer resistivity $\sim T^{-1.5}$) core plasma connects to the insulating vacuum through a boundary layer where temperatures are much lower. The layer where neither the ideal plasma nor the ideal vacuum approximation may be applied is generally thin enough[42,55] that treating it as an abrupt transition provides a reasonable approximation. These models place the plasma-vacuum transition slightly inside of the nominal separatrix to avoid an ideal plasma calculation at the X point, where q diverges (and where 3D effects are important such that the 2D equilibrium approximation breaks down). That is, the ideal edge of the plasma is placed slightly inside the nominal 2D separatrix. But since q is diverging, small differences in the cutoff condition result in large differences in edge q. This makes the status of the resonance condition, $m = nq_a$, very uncertain. ELITE is able to make small adjustments to the equilibrium in order to control the value of $\Delta = (m_0 - nq_a)$, where m_0 is the first m larger than nq_a. For small values of Δ, the peeling drive is larger than for higher values. Note that when a finite diamagnetic threshold is included, variation in Δ and cutoff location (when beyond $\psi_N \approx 0.994$) is generally small effects (compared to measurement uncertainty) on the calculated stability threshold.[24] Nonetheless, consistency in the treatment of these effects is required if one wishes a code benchmark to precisely reproduce calculated growth rates across different codes.

If constant Δ is not used, then variation in stability with respect to mode number n can be masked by variation in response to changing Δ. At high n, there may be many n values with similar behavior and averaging these can remove fluctuations due to changing Δ. But at low n, every step can have large effect and no averaging to remove Δ dependence is possible. In order to precisely compare stability between $n = 5$ and $n = 10$, for example, as a function of mode number, the Δ dependence must be treated consistently. ELITE can make a negligible change to the toroidal field, modifying $f^2 = (RB_\phi)^2$, in order to accommodate specified values for both cutoff location and Δ. This necessarily changes q_a slightly, but the change is well within the uncertainty. Note that because n is fairly large, the change in q_a needed to fix Δ is quite modest (e.g., for $n = 15$, changing Δ by 0.5 requires a change in q_a of $0.5/15 = 0.03$).

III. EXPERIMENT SETUP

The goal of these experiments was to test whether an ideal peeling-ballooning instability is triggering the initial transient and pedestal collapse in the H-L back transition sequence.

The case of a simple, spontaneous transition out of H-mode was isolated by establishing ELMing H-mode with NBI; during this period, type-I ELMs set the limit on pedestal height, which in turn sets the boundary conditions for core physics. The toroidal field and plasma current are held steady while the beam heating power is reduced to minimal levels needed for diagnostics, and a back transition then occurs. The back transitions examined here are furthermore distinct from cases where an actively heated H-mode plasma experiences a large type-I ELM which dissipates enough edge pressure that the plasma temporarily transitions back to L-mode before recovering into H-mode. Here, the power is low and the H-L transients are well separated in time from the periodic type-I ELMs. Typical shot parameters are listed in Table I and a typical boundary shape in relation to key diagnostics is shown in Fig. 4.

TABLE I. Typical shot parameters.

Symbol	Value	Name
B_T	2.15 T	Toroidal field
I_p	1 MA	Plasma current
β_N	1.0–2.0	Normalized beta during ELMing H-mode
q_{95}	4.6–4.9	Safety factor at 95% flux surface
κ	1.75	Elongation
δ_{up}	0.11–0.38	Upper triangularity
δ_{low}	0.3	Lower triangularity
a	0.58 m	Minor radius
R_{xpt}	1.53 m	R: major radius, dominant X point
Z_{xpt}	−1.17 m	Z: height above machine midplane, dominant X point
R_m	1.74–1.77 m	R, magnetic axis
Z_m	−0.02–0.00 m	Z, magnetic axis
$R_{gap,out}$	8.3 cm	Outer gap
P_{inj}	3300 kW (heat) 160 kW (diagnostic)	Average neutral beam power injected
V_{ac}	50, 75, 81 kV	Beam accelerating voltages for various heating and diagnostic purposes

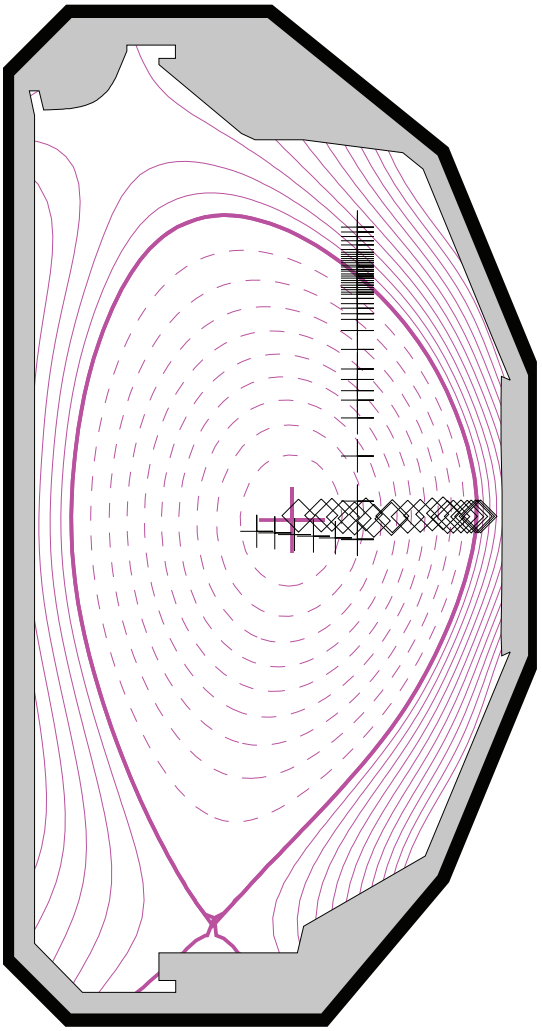

FIG. 4. EFIT equilibrium reconstruction of shot 154 749 at 4400 ms. CER chords with tangential views are marked with black diamonds. Thomson scattering chords on the core and tangential subsystems are marked with black plus signs. The separatrix is a thick magenta line. The vacuum vessel is a thick black line around the outside, and the gray area within it is taken up by equipment and carbon wall tiles.

The conditions of this experiment were arranged to make the transition sequence as long as possible to facilitate diagnosis of important phenomena and because of interest in identifying conditions for a "soft landing." To this end, a shape which has produced dithering H-L transitions in previous experiments was chosen. Although long dithering phases are present in the transition sequences examined, the start of the sequence is still associated with a large, ELM-like transient that rapidly relaxes the pedestal height (Fig. 1 at 4402 ms and Fig. 2). The dithering phase occurs after the transient. The presence of the dithering phase may be helpful in future analysis of these data as it is an essential part of some transition theories.[43,44] Note that distinction has been made between different parts of the dithering transition sequence, which can include limit cycle oscillations and type-III ELMs. Such details are irrelevant here as it is only the first spike in D_α (or rather, conditions immediately preceding it and the rapid pedestal collapse) which is being tested against P-B calculations.

In these discharges, the type-I ELMs driven during the heated phase are separated from the start of the back transition sequence by a long ELM-free period lasting up to hundreds of milliseconds (about 170 ms in the example of Fig. 1). During this time, low powered neutral beams are used to enable measurements of carbon ion impurity temperature, density, and rotation with CER. The ion profiles were combined with electron profiles and used to reconstruct kinetic equilibria with EFIT.

Similar magnetic signals have been detected in association with both type-I ELMs and back transition transients, including observation of spikes in $\dot{B}$ corresponding to the spikes in D_α and roughly 100 μs of precursor activity before the spike. However, the DIII-D magnetics system cannot resolve mode numbers higher than $n = 4$,[18] compared to $n \sim 5 - 30$ for typical ELMs. No clear distinction between ELMs and back transition transients has been found using magnetics data, and these data do not prove that these events are triggered by the same mechanism.

IV. STABILITY ANALYSIS

Kinetic EFITs were constructed from data taken ~10 ms before the transient events at the start of back transition sequences. The exact timing varied from case to case and the preferred candidates for analysis were those with neutral beam blips supplying CER data in close temporal proximity to the start of the events. Use of at least two CER time slices was preferred to improve accuracy. With a 2.5 ms CER integration time and 5 ms beam blips, this usually meant one blip was needed, but there were occasions where data from two blips were needed. In such cases, the time period from which data was drawn extended to ≈20 ms before the start of the back transition. Such a long time period is acceptable given the slow evolution of the discharge preceding the back transition, with ELM-free periods commonly persisting for more than 100 ms between the last type-I ELM and the start of the H-L sequence. The EFITs were calculated for 257×257 R-Z grids.

Each kinetic EFIT was used as a basis for a set of variations in edge current density and pressure gradient. The profiles in the core are adjusted to maintain constant total current I_p and β_p. For a well-constructed initial kinetic EFIT and reasonable range of variation, most ($\gtrsim 90\%$) of the perturbed EFITs typically converge. A set of about 200 perturbation points give a fairly well resolved view of stability in $p' - J$ space and allow easy identification of outliers, which are then removed.

For the purposes of labeling the profiles, p' is evaluated at the location of peak pressure gradient. The current label J is intended to give a sense of the amount of current at the edge of the plasma and is the average of current density at the bootstrap peak and at the "separatrix" (after cutoff) normalized to the average current density throughout the plasma. The full pressure and current profiles output by the equilibrium reconstruction are used by ELITE.

ELITE is used to calculate a growth rate for each point in the $p' - J$ scan for each of a selection of mode numbers. $n = 5$, 10, 15, 20, and 25 were tested for all cases, giving a good representation of the overall stability boundary. The majority of runs were performed with a cutoff at 99.5% of ψ_N. The resonance control was set to $\Delta = m_0 - nq_a = 0.2$, where q_a is the safety factor at the last closed flux surface and m_0 is the poloidal mode number of the resonant surface just outside the plasma, such that $0 \leq \Delta < 1$. The choice of $\Delta = 0.2$ was used, consistent with prior ELITE studies, to avoid resonance effects associated with Δ very near 0 or 1, and to give a typical value of the growth rate averaged over possible values of Δ. For intermediate to high-n modes, Δ is not a measured quantity (within measurement uncertainty), and the physical significance of resonant effects is unclear due to the presence of a separatrix.

A more tightly converged EFIT was generated for one case and a test with ELITE found insignificant difference in the boundary locations, demonstrating that the standard convergence level used in the rest of the runs was adequate. A cutoff at 99.7% of ψ_N was tested and found to also have insignificant effect on the boundary location, consistent with expectations.

Use of ELITE in this work is within the typical range of expected accuracy. On the one hand, ELITE is often used to calculate stability in long periods of steady operation,[45] where the availability of many time-slices reduces uncertainty. On the other hand, ELITE has also been used to analyze stability in successive time windows with limited data available for each window.[7] Analysis of stability before a back transition is similar to one such window, but this work benefits from recent diagnostic improvements,[12,18] which substantially improve the data quality obtainable from each single time-slice while increasing the sampling frequency. The transient nature of the event at the start of the H-L transition sequence is no different than the transient nature of an ELM. In fact, the quiescent period prior to the H-L sequence is much longer than the typical inter-ELM time; if anything, this study should suffer less error due to evolving parameters. Finally, the challenges of properly fitting and aligning profiles during the profile fitting process have been identified as the dominant source of error in ELITE calculations, meaning that most ELITE use cases should experience similar levels of uncertainty given similar profile quality.

As further verification that data quality was adequate and the analysis procedure and setup were valid, ELITE was used to analyze conditions not just before back transitions, but also before ELMs and shortly after the L-H transition, as seen in Fig. 5. ELMing H-mode was analyzed by conditionally averaging data based on ELM-phase. Measurements were accepted if they occurred between 80% and 99% of the time interval between any two ELMs and rejected otherwise. This is based on the observation that most of the inter-ELM recovery of the pedestal is rapid and the profiles are nearly fully developed by 80% of the inter-ELM time. So, the plasma should be very close to peeling-ballooning instability by this time. In the window chosen between the L-H transition and the first ELM, it can be clearly seen that the pedestal has not developed enough to trigger ELMs. These (ELM-free and ELMing) cases were used to validate the data and procedures being used.

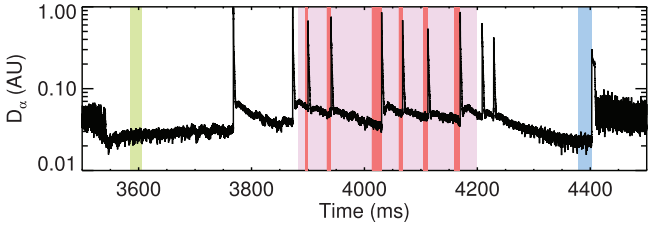

FIG. 5. Time trace of D_α emission at the outer strike point shaded to show the data selection windows for a set of ELITE runs. Shaded in green at the left is an early ELM-free period after the L-H transition. Shaded in pale pink is the overall time window where consideration of ELMs was allowed. The window starts late in an attempt to capture ELMs with consistent properties such as inter-ELM period. The window ends when NBI power is reduced. In red are the windows where the 80%–99% criterion was satisfied and data were used. Shaded in blue is the pre-H-L transition time window.

Calculations with ELITE clearly show the plasma evolving from a condition of P-B stability shortly after the L-H transition, to a condition of P-B instability before each type-I ELM, and back to stability before the H-L transition sequence begins with the transient. Example stability maps for these three cases are shown in Figs. 6–8 with the same plot ranges. See Fig. 5 for the data selection windows corresponding to the stability maps below. The normalized pressure gradient α, used as the X axis of these figures, is given by $\alpha = (2\mu_0/4\pi^2)(dp/d\psi)(dV/d\psi)\sqrt{(V/2\pi^2 R)}$ for general magnetic geometry.[46,47] In simplified, shifted circle geometry, it would be $\alpha = -Rq^2 d\beta/dr$; compare with the approximate condition for ballooning instability given earlier: $(d\beta/dr) \sim (1/Rq^2)$.[27] It can be seen from Figs. 6 and 7 that ELITE is predicting stability and instability in the early ELM-free and ELMing validation cases consistent with earlier published results.[7,24] Figure 8 shows that the plasma is stable before the back transition: the large D_α transient event is not an intermediate-n ideal peeling ballooning mode and so it is not a type-I ELM.

Figure 9 repeats the data shown in Fig. 8 with the grid points marked by their most unstable toroidal mode number, showing that $n = 5$ is common near the peeling boundary and $n = 6 - 8$ is more common near the "nose," with a trend

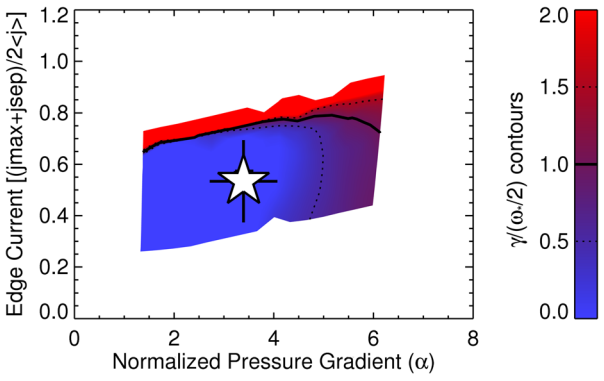

FIG. 6. Stability diagram for the plasma in ELM-free operation shortly after the completion of the L-H transition sequence. The thick black line shows the boundary between stable and unstable territory in $p' - J$ space, defined by $\gamma = \omega_*/2$, where γ is the uncorrected ideal MHD growth rate. The operating point, marked by a white star, is well within stable territory.

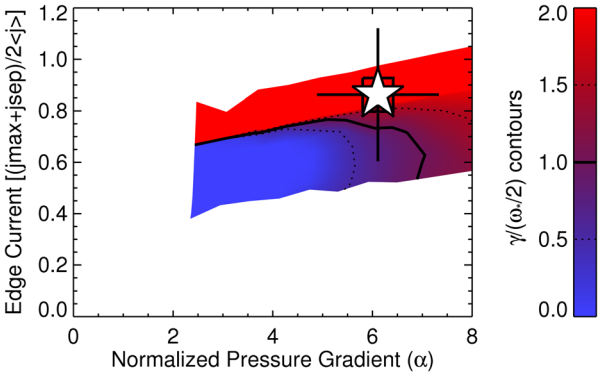

FIG. 7. Stability diagram for 80%–99% of the ELM cycle for the same H-mode as in Fig. 6. The difference between the operating point and the stability boundary is less than the estimated uncertainty, consistent with operation near the onset of peeling-ballooning instability.

towards higher n as current decreases along the ballooning boundary at the right.

Figure 10 shows the boundaries from Figs. 6–8 overlaid. There is a minor difference between the peeling boundary between the ELMing and non-ELMing cases (top boundary, nearly horizontal, approached as edge current increases). There is another difference between the pre-HL and ELMing boundaries at the "nose" of the diagram in the upper right; the ballooning boundary for the ELMing case extends to higher α. However, if the shallow gradient of growth rate in this region (see spacing of dashed lines in Fig. 8) is interpreted as uncertainty in the ballooning boundary, then the difference in ELMing and pre-HL boundaries is not very significant.

The relative stability boundary position between the ELMing and pre-transition cases (red dashed line vs. blue solid line in Fig. 10) is important because changes in the boundary are harder to detect from simple measurements than are changes in pedestal height. It could be seen from automatic tanh fits to the pedestal profile that the electron pressure gradient was not evolving dramatically during the ELM-free period following power reduction, and the gradient was lower throughout the ELM-free period than it was before the ELMs. Although the ion behavior is less obvious, it still could be reasonably expected that the ballooning limit was not being reached by evolution of the pressure gradient.

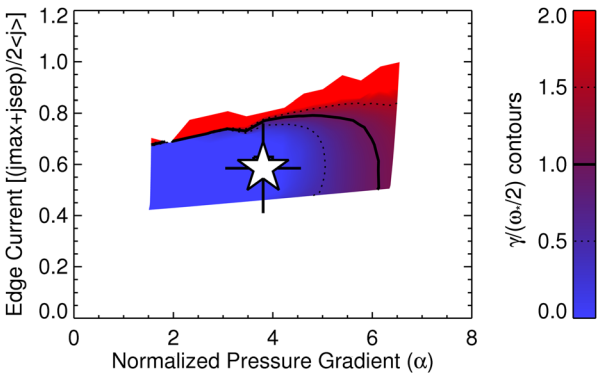

FIG. 8. Pre-H-L back transition stability diagram. The operating point has returned to stable space. The current error bar nearly reaches the boundary, but falls just short.

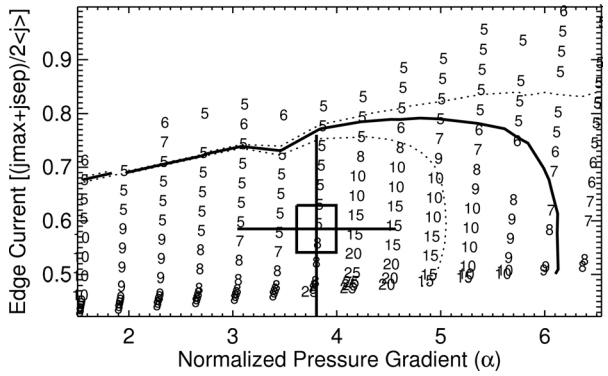

FIG. 9. Pre-H-L back transition stability diagram, showing the distribution of test points in the $p' - J$ perturbation scan. $\gamma = \omega_*/2$ is marked by a thick line with thin dashed lines at 0.5 and 1.5 times this value. The numbers on the plot indicate the mode with the highest growth rate γ at each test point (γ may be below the stabilization threshold). Tested were $n = 5 - 10$, 15, 20, 25.

However, the hypothesis that the boundary was contracting to meet the operating point seemed reasonable prior to these calculations. The change in the calculated ballooning limit is small compared to the difference between boundary and the operating point, so clearly it is not the case that a ballooning dominated mode is being triggered by a contracting stability boundary at the time of the H-L back transition transient.

Note that it is also possible for a ballooning mode to be triggered by a decrease in current if the pressure gradient is maintained (Fig. 3) because edge current has a stabilizing effect on the ballooning mode. It can be seen from the ELITE results (Fig. 8) that this triggering mechanism is not responsible for the transient. A ballooning mode triggered by reduction in current might happen with stronger shaping of the plasma boundary because shaping tends to produce a ballooning boundary with a shallower positive slope vs. pressure gradient.

The peeling behavior is less obvious. The lowest order expectation from time traces of easily diagnosed quantities would be that edge current is decreasing, as electron pressure gradient is fairly steady while density accumulates, increasing collisionality. So, in order to trigger a peeling dominated mode, the current limit would have to decrease faster than the edge current. The comparison in Fig. 10 shows that the

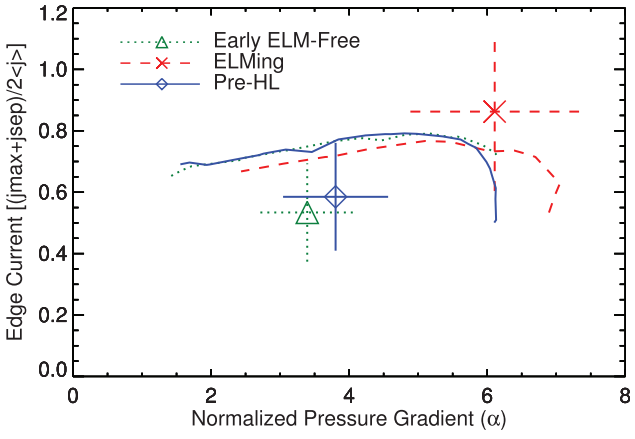

FIG. 10. Overlay of the boundaries and operating points from Figs. 6–8.

boundary is not decreasing to meet the operating point; if anything, the current limit is higher before the back transition than it was during the ELMs.

The ELMing and pre-back-transition stability maps were generated across a range of values of upper triangularity. The results were consistent: the ELMing operating point was always within error bars of the boundary, and the back transition operating point was always in stable territory with error bars not reaching the boundary. None of the transient events examined were consistent with ELITE's implementation of the ideal peeling-ballooning model for $n = 5$, 10, 15, 20, or 25. All of the ELMing cases were consistent with ideal P-B instability in the same set of mode numbers.

Because the highest growth rate along much of the boundary was for the $n = 5$ mode, followed by $n = 10$, modes $n = 6 - 9$ were tested for one case. As seen in Fig. 9, $n = 5$ is dominant along the peeling boundary at the top, while n near 7 is more common at the ballooning boundary at the right. Figure 11 shows the boundaries for the mode numbers analyzed in Fig. 9. Although $n = 20$ and $n = 25$ were included in the analysis presented in this figure, their stability boundaries are so far from the operating point that the variational EFIT did not capture any point with $n = 25$ instability and only a tiny region of $n = 20$ instability is seen at the very top of the plot.

The peeling boundaries for $n = 5$ and 6 are nearly indistinguishable. The $n = 7 - 10$ boundaries are at slightly higher current, with limiting current increasing slightly with higher n. It appears that the rate of change of limiting current with n increases at higher n. At the "nose" of the diagram (the coupled peeling-ballooning region at the upper right), large expansions of the stability boundary are seen as n increases above ≈ 7, although the $n = 5 - 7$ boundaries are nearly co-located. The ballooning limit on the pressure gradient (lower right edge of stability space) contracts with increasing n from $n = 5 - 8$. The boundary expands again for $n \geq 9$, at least within the range of edge current explored in this perturbation scan. Extrapolation of the $n = 9$ and 10 boundaries would suggest that those mode numbers would be most unstable at lower current. So, the stability limit in this shot setup can be defined along much of the boundary from analyzing just the $n = 5$ mode. A good estimate across most of the boundary could be had from analysis of $n = 5$ and 10 only. The area of $p' - J$ space where $n = 6 - 9$ is limiting is small, it is far from the operating point, and the local uncertainty in boundary location is relatively large. Therefore, the analysis of $n = 5$, 10, 15, 20, and 25 only, which is what was done for all cases except for the example presented here, is sufficient to capture the stability behavior within ELITE's range of applicability, and it can be concluded that no $n \geq 5$ ideal peeling-ballooning mode is linearly unstable before any of the back transitions which were analyzed.

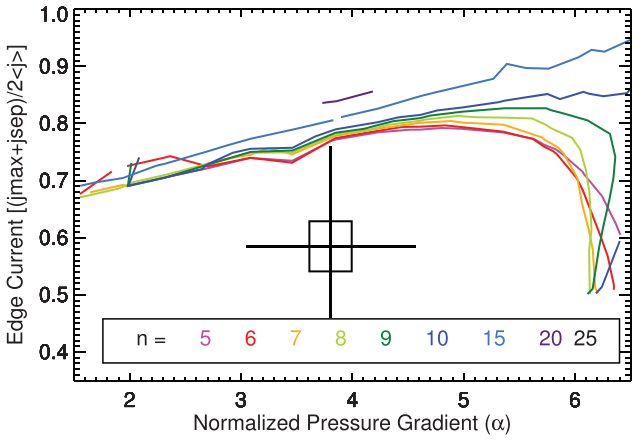

FIG. 11. Overlay of the boundaries of several mode numbers present in the analysis shown in Fig. 9.

V. OTHER TESTS

A. Triangularity scan

A scan in triangularity was included as a test of parametric dependencies in P-B theory: theory[7] and experiment[3] agree that the limiting pressure gradient before large type-I ELMs should depend on the plasma triangularity opposite to the dominant X point. Thus, if the H-L transients of interest here are large type-I ELMs, they both should then have the same scaling of critical p' with triangularity. The upper triangularity of these lower single-null discharges was scanned from 0.11 to 0.39 (Fig. 12) to allow comparison of the pre-back-transition pressure gradient to the pre-ELM pressure gradient to provide a secondary experimental check on the results from ELITE.

To maximize the number of back transitions observed in this scan, the primary heating power was cycled on and off, resulting in a series of transitions in and out of H-mode, as seen in Fig. 13. In fact, not all of the transitions proceeded all the way to L-mode, but rather, H-I-H sequences were common, where I stands for I-phase and represents the dithering part of the transition sequence. This is acceptable as the I-L transition occurs at low stored energy and pedestal height and has always been observed to go smoothly. The ELM-candidates occur at the H-I transition. The difference between the H-I-L-I-H and H-I-H sequences is therefore irrelevant to this study.

The first period of H-mode in the example shot is different from some of the others which follow. There was not

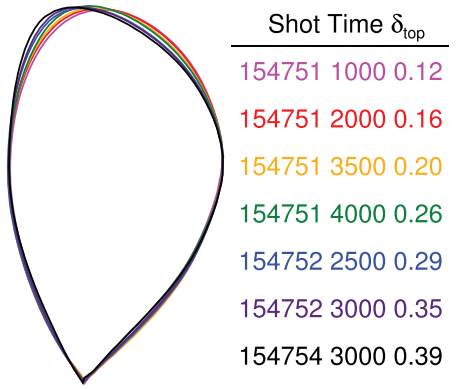

FIG. 12. Variation of upper triangularity: the plasma boundary is shown at several representative time slices during the triangularity scan. Note the difference in the top left corner of the boundary.

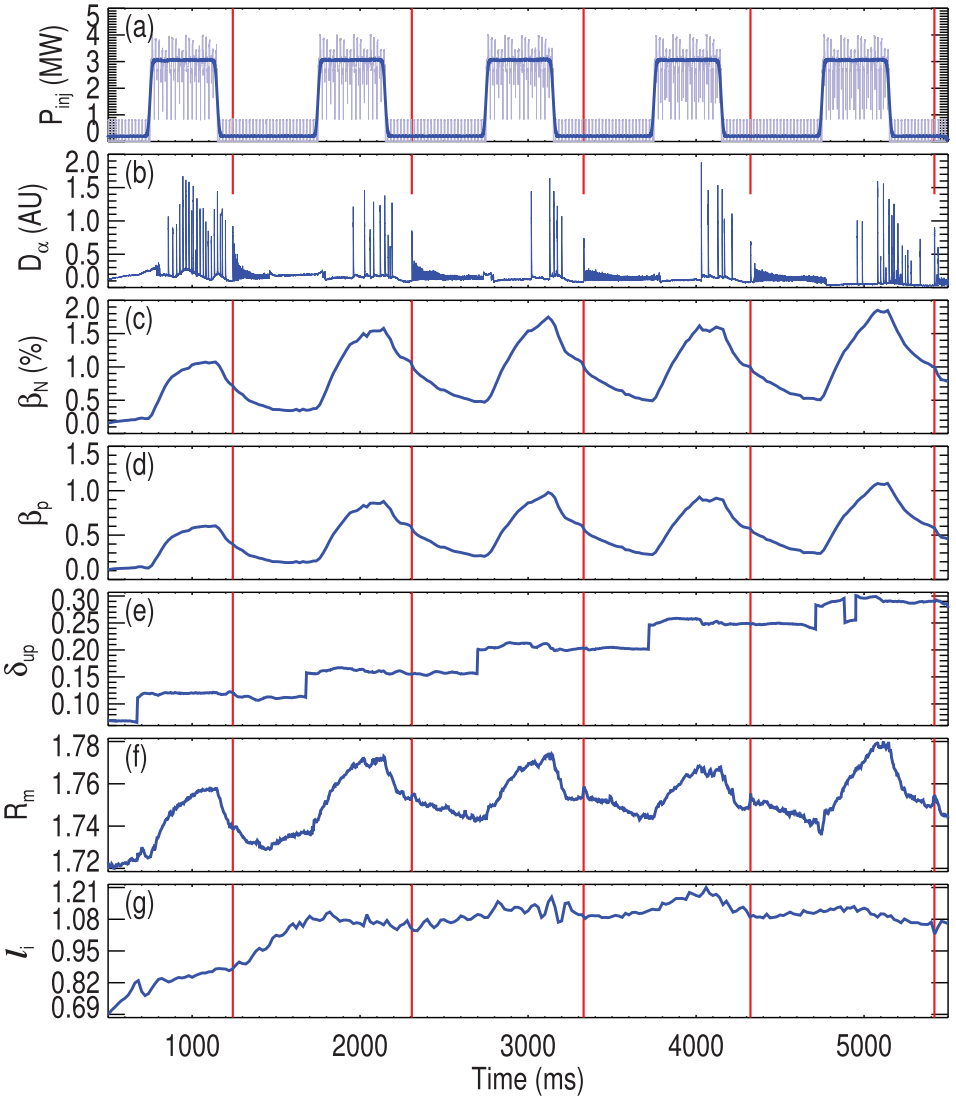

FIG. 13. Setup of a typical shot, including several transitions in and out of H-mode for the upper triangularity scan. Vertical red lines mark the start times of five back transition sequences, each beginning with an ELM-like transient. (a) Neutral beam injected power, (b) divertor D_α emission, (c) β_N, (d) β_p poloidal beta, (e) δ_{up}: upper triangularity, (f) R_m: major radius of magnetic axis, (g) l_i: internal inductance, showing that the first H-mode was not fully relaxed. The traces shown in Fig. 1 correspond to one of the phases of H-mode in a similarly constructed shot.

enough time allowed for the current profile to fully relax. That the core current profile is not fully relaxed is reflected in l_i measured at ≈75% of the value seen in the following H-modes. Full current profile relaxation appears to be achieved in the second H-mode. These early H-modes appear to display the same transient at the start of the back transition sequence as do later H-phases, and tests with ELITE in one of these cases were consistent with tests on the later, higher l_i cases: the plasma is P-B unstable during the ELMing phase and P-B stable before the H-L transition.

Figure 14 shows the results of the triangularity scan. Each back transition was preceded by a period of ELMing H-mode. The maximum pressure gradient observed between ELMs is shown in black and the maximum pressure gradient observed between the last ELM and the start of the back transition is shown in red. Here, the pressure gradient is defined by the ratio of height to width of a series of hyperbolic tangent fits to the electron pressure measurements made by Thomson scattering and adjusted to account for flux expansion such that the reported pressure gradient should be equivalent to a measurement made at the outboard midplane. The tanh fit is performed using positions of chords along the vertical laser, shown in Fig. 4. The details of the tanh fit to the pedestal are described in Ref. 48. Upper triangularity is calculated from the geometry of the EFIT.[16,47,49]

Linear fits to each group of data show that the maximum pressure gradient before ELMs increases with triangularity with a slope of 1078 ± 91 kPa/m, whereas the maximum pressure gradient before back transitions varied with a slope of 431 ± 65 kPa/m. Thus, the pre-ELM critical electron pressure gradient needed for ELM onset increases 2.5 ± 0.43 times faster than pre-transition gradient when upper triangularity is increased in the range of $0.1 < \delta_{top} < 0.4$.

The significantly different dependence on triangularity between the pre-ELM and pre-transition cases shows that the pressure gradient before the transition is not being limited by the same mechanism (ideal P-B instability) as before the type-I ELMs. This is consistent with the conclusion of the ELITE tests in Sec. IV that the back transition transient is not a type-I ELM. Note that very large type-I ELMs often occur near the "nose" of the stability diagram [in general[7] and in these experiments, see Fig. 7], where peeling-ballooning coupling is important. The largest type-I ELMs are typically strongly coupled peeling-ballooning modes. Smaller ELMs may be produced by crossing other parts of the P-B boundary. A ballooning dominated ELM, for

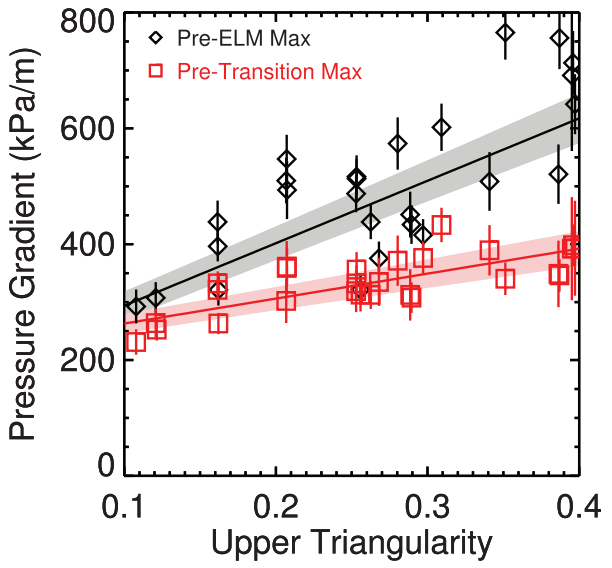

FIG. 14. Pressure gradients vs. upper triangularity. Black diamonds: maximum gradient measured during ELMs for each H-mode. Red squares: maximum gradient observed during the ELM-free phase before each back transition. The gradient here is calculated from the height and width of a hyperbolic tangent fit to electron pressure. Width is adjusted for flux expansion and geometry to give the gradient at the outboard midplane. The lines are linear fits to the two datasets and the shaded regions represent uncertainty in the fits.

example, could relax its own drive (pressure gradient) and turn itself off fairly quickly.[7] So, the difference in ∇p vs. δ_{top} scaling with does not prove that these plasmas are stable to ideal peeling or ballooning before back transitions, but it does indicate that strongly coupled peeling-ballooning activity is not at work in the H-L transitions, again consistent with the conclusion that back transition associated transients are not large type-I ELMs.

B. Radial structure of pedestal collapse

The normalized temperature loss profile $\Delta T_e/T_e = (T_{e,final} - T_{e,initial})/T_{e,initial}$ across ELMs has been shown to be a good estimator for mode structure and is consistent with calculated mode amplitude profiles.[7,8] Figure 15 compares the temperature losses across an example ELM (left) and a back transition transient (right). The top row shows electron temperature profiles measured by Thomson scattering before and after each event, followed by the differences in the before and after profiles on the second row. The timing of the profiles relative to the spikes is shown at the bottom of the figure. Evolution of plasma parameters is typically much faster after a crash than before: in an ELMing H-mode, most of the recovery happens early in the inter-ELM period. So it is critical that the timing between the "after" profiles and the D_α spikes be similar and cases with similar timing were found. The "before" profile is much less sensitive to timing, provided it is not within the short ($\sim$1–10 μs) growth time of the MHD mode that triggers the ELM crash.

Figure 15(e) shows the normalized temperature losses from both the ELMing (blue triangle) and back transition (purple square) example cases overlaid. It is seen that the ELM effects penetrate farther than the HL transient, which is more narrowly localized within the edge barrier region. Thus, the transient associated with the back transition has a different radial mode structure than a typical type-I ELM, suggestive of a different physical mechanism behind each, which is consistent with the other results showing that the back transition transients are not type-I ELMs.

VI. DISCUSSION

Experiments were performed to facilitate analysis of the large transient seen at the start of H-L back transition sequences: NBI heating power was reduced to the minimum level required for diagnostics (edge CER), while other parameters, such as plasma current and toroidal field, were held steady. This produced discharges where the start of the back transition sequence was separated in time from the typical type-I ELMing period of the discharge. The plasma boundary shape was chosen to produce dithering H-L transitions, as the dithering transition is a candidate for producing a "soft landing" wherein stored energy ramps down smoothly, rather than suffering a sudden drop as in a "hard" back transition. However, even with a setup which produces long, slow, dithering transitions, the H-L sequence still normally begins with the transient: hard back transitions happen even when the rest of the transition sequence is very gradual. This is a barrier to engineering a soft landing, which motivated studies in these particular conditions and this shape.

The results presented here show that the back-transition transient in these shots is not driven by the same physics as the large type-I ELMs it resembles: it is not a linear, ideal peeling-ballooning instability and it is especially not a peeling-ballooning mode triggered near the "nose" of the stability diagram, as is typical of large type-I ELMs. This conclusion is supported by three findings.

First, results from linear MHD stability analysis using ELITE clearly show that the triggering mechanism for the transient at the start of these H-L transition sequences is not an $n \geq 5$ ideal peeling-ballooning instability, although resistive, kinetic, and nonlinear effects are not ruled out. In particular, the stability maps in Figs. 6–11 and the history of pressure gradients in Fig. 1 show that, just prior to the start of the H-L transition sequence, the plasma operating point is well away from the ballooning boundary and is not evolving toward it: increases in pressure gradient are clearly not triggering a ballooning dominated mode. Second, the difference in the scaling of the maximum pressure gradient before ELMs and back transitions vs. boundary shape is quite different. If the back transition transient was due to the same physics as found in type-I ELMs, then the scaling in the two cases should be similar. It is true that the error bars on the operating point on the stability maps are large in the vertical direction and nearly reach the peeling stability boundary (Fig. 8). However, during the ELM-free period prior to the back transition, the density is increasing and temperature is decreasing at the edge, which means that collisionality $\nu_* \sim n/T^2$ is increasing and bootstrap current should thus decrease.[22] This then implies that the plasma operating point is moving down in the stability plot (e.g., Fig. 8) away from the peeling boundary. As a result, it seems quite implausible that instability could

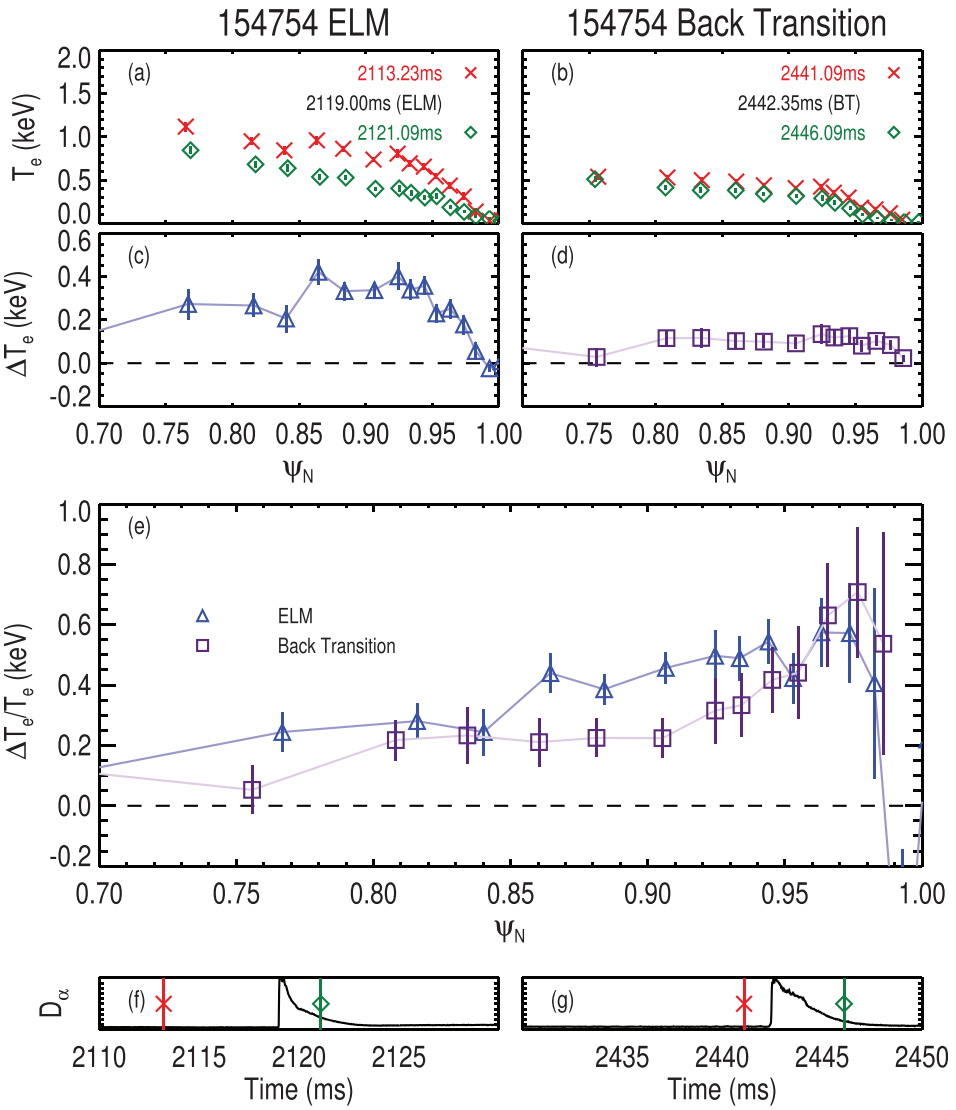

FIG. 15. Changes in electron temperature profile from Thomson scattering before and after a typical type-I ELM (left) and a back transition transient (right) showing differences in mode structure: (a) and (b) temperature profiles before (red X) and after (green diamond) the event in question, (c) and (d) difference between profiles in first row. (e) Difference in temperature normalized to local temperature before the ELM (blue triangles) and back transition transient (purple squares), (f) and (g) time trace of D_α light from the outer strike point. Vertical lines mark the times when profiles were measured.

then be triggered by the operating point reaching the peeling stability boundary. Figure 10 shows that the stability boundary positions are fairly consistent at different times in the shot, indicating that instability is not triggered by the boundary evolving toward a stationary operating point.

Figure 11 shows that the limiting current value at fixed pressure gradient (distance between the operating point and the peeling stability boundary) decreases with n, suggesting that a lower peeling limit would be present at lower n. However, the effect of a conducting wall, which is not accounted for in ELITE, becomes increasingly important at low n: the perturbation to the vacuum field decreases with increasing poloidal mode number m (Refs. 31 and 50) and given that $m > nq_a$ for an external kink, it is clear that higher n requires higher m. A perfectly conducting wall should have a significant stabilizing effect on low n external kink modes, but less effect on higher mode numbers. A resistive wall should act like a perfectly conducting wall for modes rotating with $\omega_{\rm rot}\tau_W \gg 1$.[51,52] The typical edge toroidal rotation speed was 40–50 km/s at R = 2.2–2.3 m for these discharges and the wall penetration time in DIII-D is a few milliseconds for low n,[51,53] so $\omega_{\rm rot}\tau_W \gg 1$ is satisfied and the vacuum vessel acts like an ideal wall. Low n should then be expected to be more stable to kinking than would be suggested by an extrapolation of the ELITE results to $n < 5$. In the results shown in Fig. 11, it appears that $n = 5$ and $n = 6$ have essentially identical peeling limits, with $n = 7 - 10$ only slightly higher. This trend suggests a $n = 1$ boundary very close to the $n = 5$ boundary in the no-wall limit, with an even higher limiting current after wall stabilization is accounted for. Therefore, low $n < 5$ external kinks should not be expected to be unstable in these cases.

Finally, a third observation supporting our conclusion is the fact that lower n modes typically penetrate deeper into the plasma,[8] yet the H-L transient perturbation shown in Fig. 15 shows shallower penetration depth than the type-I ELMs, indicating that the transient has a higher n than do the type-I ELMs, which are consistent with $n = 5 - 10$ P-B instability. Thus, the back transition transient is likely not due to $n < 5$ P-B instability. This is consistent with preliminary GATO[36] results, which so far do not indicate any $n < 5$ unstable modes, but a detailed discussion of low-n stability is deferred to future work.

When the P-B coupling is reduced by strong shaping, the stabilizing effect of edge current on ballooning modes dominates the slope of the ballooning boundary (Fig. 3) and

it should be possible to trigger a ballooning dominated mode by decreasing edge current, while holding pressure gradient constant. This is qualitatively consistent with what is observed: the pressure gradient does not change much during the pre-HL ELM-free period [Fig. 1(f)], but temperature [Fig. 1(e)] decreases while density [Fig. 1(d)] increases, implying decay of the bootstrap current. However, the nose of the calculated stability diagrams does not appear to be prominent enough to support this as a mechanism for the H-L back transition event, nor is the pressure gradient prior to the transition high enough (the operating point doesn't start in the nose, so it cannot exit the nose by moving to lower current). Furthermore, the lowest values in the triangularity scan had no sign of the "overhang" in the stability boundary (formed by positive slope of the ballooning boundary as seen in Fig. 3) which would allow this phenomenon: the stabilizing effect of edge current on the ballooning mode was negated by coupling between peeling and ballooning, and the ballooning limited pressure gradient decreased with more current. The transients were still observed in these low triangularity cases. This rules out the last possible path across the boundary and eliminates ideal peeling-ballooning as an explanation for the observed transient.

Having eliminated type-I ELM like events as the trigger for the prompt H-L back transition, we are then left searching for an alternate explanation. We note that during the ELM-free period before the start of the back transition sequence, the electron pressure gradient was not found to decay significantly in these experiments. Pedestal density rises significantly while temperature falls, resulting in increasing resistivity in the pedestal. These conditions could be driving a resistive instability. High density type-III ELMs, thought to be associated with resistive instabilities, are an example of ELM-like phenomena which occur below the zero resistivity peeling-ballooning boundary;[7] thus, it is possible that the D_α burst associated with the start of the back transition sequence is related to this type of resistive MHD phenomena. A more detailed analysis of this possibility requires further work.

As mentioned earlier, H-mode is sustained by a sufficiently strong $E \times B$ shear at the plasma boundary. Thus, another possible explanation for the abrupt drop in pedestal height at the start of the back transition is an abrupt failure of shear suppression of turbulence. If shear in the $E \times B$ drift velocity, which is normally responsible for suppressing turbulence in H-mode pedestals, were to decay, recovering turbulence would be expected to drive more transport, erode the pedestal more, and further reduce $v_{E\times B}$ shear. If this feedback loop were able to quickly reduce edge density and pressure to L-mode levels, it might manifest as a sudden expulsion of heat and particles, causing a drop in stored energy, pedestal height, and a flash of light as the ejecta cool and hit the divertor targets. Data taken during this experiment with CER and beam emission spectroscopy[54] enable tests of this hypothesis, which are being reported in a separate publication.

VII. CONCLUSION

Tests with ELITE have shown that the event which commonly initiates the H-L transition sequence in shots where heating power is removed while other parameters (I_p, B_T, etc.) are held steady is not driven by an ideal peeling-ballooning instability and is therefore distinct from the type-I ELMs which commonly occur in strongly heated H-mode. This conclusion is also supported by a significant difference in scaling with boundary shape between the ELM-limited pressure gradient and the pre-transition pressure gradient and by differences in radial penetration of these events as inferred from changes in temperature profiles. Future work will characterize fluctuations around the time of the back transition and examine the hypothesis that the H-L transition sequence begins when the shear in the $E \times B$ flow becomes too weak to maintain turbulence suppression.

ACKNOWLEDGMENTS

This material is based upon work supported in part by the U.S. Department of Energy, Office of Science, Office of Fusion Energy Sciences, using the DIII-D National Fusion Facility, a DOE Office of Science user facility, under Award Nos. DE-FC02-04ER54698, DE-FG02-07ER54917, DE-AC02-09CH11466, and DE-FG02-08ER54984. DIII-D data shown in this paper can be obtained in digital format by following the links at https://fusion.gat.com/global/D3D_DMP.

[1]F. Wagner, G. Becker, K. Behringer, D. Campbell, A. Eberhagen, W. Engelhardt, G. Fussmann, O. Gehre, J. Gernhardt, G. von Gierke, G. Haas, M. Huang, F. Karger, M. Keilhacker, O. Klüber, M. Kornherr, K. Lackner, G. Lisitano, G. G. Lister, H. M. Mayer, D. Meisel, E. R. Müller, H. Murmann, H. Niedermeyer, W. Poschenrieder, H. Rapp, H. Röhr, F. Schneider, G. Siller, E. Speth, A. Stäbler, K. H. Steuer, G. Venus, O. Vollmer, and Z. Yü, Phys. Rev Lett. **49**, 1408 (1982).
[2]K. H. Burrell, Plasma Phys. Controlled Fusion **36**, A291 (1994).
[3]T. H. Osborne, J. R. Ferron, R. J. Groebner, L. L. Lao, A. W. Leonard, M. A. Mahdavi, R. Maingi, R. L. Miller, A. D. Turnbull, M. Wade, and J. Watkins, Plasma Phys. Controlled Fusion **42**, A175 (2000).
[4]G. Federici, P. Andrew, P. Barabaschi, J. Brooks, R. Doerner, A. Geier, A. Herrmann, G. Janeschitz, K. Krieger, A. Kukushkin, A. Loarte, R. Neu, G. Saibene, M. Shimada, G. Strohmayer, and M. Sugihara, J. Nucl. Mater. **313–316**, 11 (2003).
[5]A. Loarte, M. Sugihara, M. Shimada, A. Kukushkin, D. Campbell, M. Pick, C. Lowry, M. Merola, R. A. Pitts, V. Riccardo, G. Arnoux, W. Fundamenski, G. F. Matthews, S. Pinches, A. Kirk, E. Nardon, T. Eich, A. Herrmann, G. Pautasso, A. Kallenbach, G. Saibene, G. Federici, R. Sartori, G. Counsell, A. Portone, M. Cavinato, M. Lehnen, A. Huber, V. Philipps, D. Reiter, V. Kotov, R. Koslowski, G. Maddaluno, B. Lipschultz, D. Whyte, B. LaBombard, R. Granetz, A. Leonard, M. Fenstermacher, E. Hollman, P. C. Stangeby, M. Kobayashi, R. Albanese, G. Ambrosino, M. Ariola, G. de Tommasi, J. Gunn, M. Becoulet, L. Colas, M. Goniche, E. Faudot, and D. Milanesio, in the *Proceedings of the 22nd IAEA Fusion Energy Conference, Geneva, Switzerland* (2008); see http://www-pub.iaea.org/MTCD/Meetings/fec2008/it_p6-13.pdf.
[6]A. Loarte, G. Huijsmans, S. Futatani, L. R. Baylor, T. E. Evans, D. M. Orlov, O. Schmitz, M. Becoulet, P. Cahyna, Y. Gribov, A. Kavin, A. Sashala Naik, D. J. Campbell, T. Casper, E. Daly, H. Frerichs, A. Kischner, R. Laengner, S. Lisgo, R. A. Pitts, G. Saibene, and A. Wingen, Nucl. Fusion **54**, 033007 (2014).
[7]P. B. Snyder, H. R. Wilson, J. R. Ferron, L. L. Lao, A. W. Leonard, T. H. Osborne, A. D. Turnbull, D. Mossessian, M. Murakami, and X. Q. Xu, Phys. Plasmas **9**, 2037 (2002).
[8]A. D. Turnbull, L. L. Lao, T. H. Osborne, O. Sauter, E. J. Strait, T. S. Taylor, M. S. Chu, J. R. Ferron, C. M. Greenfield, A. W. Leonard, R. L. Miller, P. B. Snyder, H. R. Wilson, and H. Zohm, Plasma Phys. Controlled Fusion **45**, 1845 (2003).
[9]D. N. Hill and the DIII-D Team, Nucl. Fusion **53**, 104001 (2013).
[10]K. H. Burrell, Phys. Plasmas **4**, 1499 (1997).
[11]D. M. Thomas, R. J. Groebner, K. H. Burrell, T. H. Osborne, and T. N. Carlstrom, Plasma Phys. Controlled Fusion **40**, 707 (1998).

[12]D. M. Thomas, R. J. Groebner, T. H. Osborne, T. W. Petrie, K. H. Burrell, and T. N. Carlstrom, "Scaling of the back transition and dynamical tests of theory on DIII-D," presented at the *7th IAEA Technical Committee Meeting on H-Mode Physics and Transport Barriers, Oxford*, UK (1999).
[13]P. A. Politzer, G. L. Jackson, D. A. Humphreys, T. C. Luce, A. W. Hyatt, and J. A. Leuer, Nucl. Fusion **50**, 035011 (2010).
[14]V. Parail, R. Albanese, R. Ambrosino, J.-F. Artaud, K. Bessenghir, M. Cavinato, G. Corrigan, J. Garcia, L. Garzotti, Y. Gribov, F. Imbeaux, F. Koechl, C. V. Labate, J. Lister, X. Litaudon, A. Loarte, P. Maget, M. Mattei, D. McDonald, E. Nardon, G. Saibene, R. Sartori, and J. Urban, Nucl. Fusion **53**, 113002 (2013).
[15]A. Loarte, F. Koechl, M. J. Leyland, A. Polevoi, M. Beurskens, V. Parail, I. Nunes, G. R. Saibene, R. I. A. Sartori, and JET EFDA Contributors, Nucl. Fusion **54**, 123014 (2014).
[16]L. L. Lao, H. St. John, R. D. Stambaugh, A. G. Kellman, and W. Pfeiffer, Nucl. Fusion **25**, 1611 (1985).
[17]E. J. Strait, Rev. Sci. Instrum. **77**, 023502 (2006).
[18]J. D. King, E. J. Strait, R. L. Boivin, D. Taussig, M. G. Watkins, J. M. Hanson, N. C. Logan, C. Paz-Soldan, D. C. Pace, D. Shiraki, M. J. Lanctot, R. J. La Haye, L. L. Lao, D. J. Battaglia, A. C. Sontag, S. R. Haskey, and J. G. Bak, Rev. Sci. Instrum. **85**, 083503 (2014).
[19]D. Eldon, B. D. Bray, T. M. Deterly, C. Liu, M. Watkins, R. J. Groebner, A. W. Leonard, T. H. Osborne, P. B. Snyder, R. L. Boivin, and G. R. Tynan, Rev. Sci. Instrum. **83**, 10E343 (2012).
[20]K. H. Burrell, P. Gohil, R. J. Groebner, D. H. Kaplan, J. I. Robinson, and W. M. Solomon, Rev. Sci. Instrum. **75**, 3455 (2004).
[21]D. M. Thomas, G. R. Mckee, K. H. Burrell, F. Levinton, E. L. Foley, and R. K. Fisher, Fusion Sci. Technol. **53**, 487 (2008).
[22]O. Sauter, C. Angoni, and Y. R. Lin-Liu, Phys. Plasmas **6**, 2834 (1999).
[23]O. Sauter, C. Angoni, and Y. R. Lin-Liu, Phys. Plasmas **9**, 5140 (2002).
[24]P. B. Snyder *et al.*, Nucl. Fusion **49**, 085035 (2009).
[25]F. L. Hinton and R. D. Hazeltine, Rev. Mod. Phys. **48**, 239 (1976).
[26]F. F. Chen, *Plasma Physics and Controlled Fusion* (Plenum Press, New York, 1984), Vol. 1, p. 199.
[27]J. Wesson, *Tokamaks* (Oxford University Press, New York, 1987), p. 137.
[28]E. A. Frieman, J. M. Greene, J. L. Johnson, and K. E. Weimer, Phys. Fluids **16**, 1108 (1973).
[29]J. W. Connor, R. J. Hastie, H. R. Wilson, and R. L. Miller, Phys. Plasmas **5**, 2687 (1998).
[30]H. R. Wilson, P. B. Snyder, G. T. A. Huysmans, and R. L. Miller, Phys. Plasmas **9**, 1277 (2002).
[31]J. Wesson, Nucl. Fusion **18**, 87 (1978).
[32]P. B. Snyder, K. H. Burrell, H. R. Wilson, M. S. Chu, M. E. Fenstermacher, A. W. Leonard, R. A. Moyer, T. H. Osborne, M. Umansky, W. P. West, and X. Q. Xu, Nucl. Fusion **47**, 961 (2007).
[33]C. C. Hegna, J. W. Connor, R. J. Hastie, and H. R. Wilson, Phys. Plasmas **3**, 584 (1996).
[34]K. V. Roberts and J. B. Taylor, Phys. Rev. Lett. **8**, 197 (1962).
[35]P. B. Snyder, G. J. Groebner, J. W. Hughes, T. H. Osborne, M. Beurskens, A. W. Leonard, H. R. Wilson, and X. Q. Xu, Nucl. Fusion **51**, 103016 (2011).
[36]L. C. Bernard, F. J. Helton, and R. W. Moore, Comput. Phys. Commun. **24**, 377 (1981).
[37]A. B. Mikhailovskii, G. T. A. Huysmans, S. E. Sharapov, and W. Kerner, Plasma Phys. Rep. **23**, 844 (1997).
[38]N. Aiba, S. Tokuda, T. Fujita, T. Ozeki, M. S. Chu, P. B. Snyder, and H. R. Wilson, Plasma Fusion Res. **2**, 010 (2007).
[39]N. M. Ferraro, S. C. Jardin, and P. B. Snyder, Phys. Plasmas **17**, 102508 (2010).
[40]G. Q. Li, X. Q. Xu, P. B. Snyder, A. D. Turnbull, T. Y. Xia, C. H. Ma, and P. W. Xi, Phys. Plasmas **21**, 102511 (2014).
[41]B. J. Burke, S. E. Kruger, C. C. Hegna, P. Zhu, P. B. Snyder, C. R. Sovinec, and E. C. Howell, Phys. Plasmas **17**, 032103 (2010).
[42]R. M. Kulsrud, *Plasma Physics for Astrophysics* (Princeton University Press, Princeton, 2005), p. 40.
[43]K. Miki, P. H. Diamond, Ö. D. Gürcan, G. R. Tynan, T. Estrada, L. Schmitz, and G. S. Xu, Phys. Plasmas **19**, 092306 (2012).
[44]L. Schmitz, L. Zeng, T. L. Rhodes, J. C. Hillesheim, W. A. Peebles, R. J. Groebner, K. H. Burrell, G. R. McKee, Z. Yan, G. R. Tynan, P. H. Diamond, J. A. Boedo, E. J. Doyle, B. A. Grierson, C. Chrystal, M. E. Austin, W. M. Solomon, and G. Wang, Nucl. Fusion **54**, 073012 (2014).
[45]P. B. Snyder, T. H. Osborne, K. H. Burrell, R. J. Groebner, A. W. Leonard, R. Nazikian, D. M. Orlov, O. Schmitz, M. R. Wade, and H. R. Wilson, Phys. Plasmas **19**, 056115 (2012).
[46]T. N. Carlstrom, K. H. Burrell, R. J. Groebner, A. W. Leonard, T. H. Osborne, and D. M. Thomas, Nucl. Fusion **39**, 1941 (1999).
[47]R. L. Miller, M. S. Chu, J. M. Greene, Y. R. Lin-Liu, and R. E. Waltz, Phys. Plasmas **5**, 973 (1998).
[48]R. J. Groebner, D. R. Baker, K. H. Burrell, T. N. Carlstrom, J. R. Ferron, P. Gohil, L. L. Lao, T. H. Osborne, D. M. Thomas, W. P. West, J. A. Boedo, R. A. Moyer, G. R. McKee, R. D. Deranian, E. J. Doyle, C. L. Rettig, T. L. Rhodes, and J. C. Rost, Nucl. Fusion **41**, 1789 (2001).
[49]W. M. Stacey and C. Bae, Phys. Plasmas **16**, 082501 (2009).
[50]X.-Z. Li, J. Kesner, and B. Lane, Nucl. Fusion **25**, 907 (1985).
[51]E. J. Strait, T. S. Taylor, A. D. Turnbull, J. R. Ferron, L. L. Lao, B. Rice, O. Sauter, S. J. Thomson, and D. Wróblewski, Phys. Rev. Lett. **74**, 2483 (1995).
[52]M. S. Chu and M. Okabayashi, Plasma Phys. Controlled Fusion **52**, 123001 (2010).
[53]M. Okabayashi *et al.*, Nucl. Fusion **45**, 1715 (2005).
[54]G. McKee, R. Ashley, R. Durst, R. Fonck, M. Jakubowski, K. Tritz, K. Burrell, C. Greenfield, and J. Robinson, Rev. Sci. Instrum. **70**, 913 (1999).
[55]Resistivity in the pedestal has not been measured directly. Length scale of exponential fit to Spitzer resistivity $\approx 2\%\psi_N \approx 0.7$ cm in H-mode; Lundquist number S (Ref. 42) with 3 cm (∼pedestal width) length scale drops to $\sim 10^4$ at $\psi_N \approx 0.99 \approx 0.3$ cm inside separatrix, compared to $>10^6$ inside of the pedestal. In fact, the region of small S is too thin to measure with Thomson scattering beyond an upper bound.